Hindawi
Journal of Nanotechnology
Volume 2019, Article ID 8235816, 11 pages
https://doi.org/10.1155/2019/8235816

Research Article

Effect of Temperature and Capping Agents on Structural and Optical Properties of Tin Sulphide Nanocrystals

Abimbola E. Oluwalana and Peter A. Ajibade

School of Chemistry and Physics, University of KwaZulu-Natal, Private Bag X01, Scottsville, Pietermaritzburg 3209, South Africa

Correspondence should be addressed to Peter A. Ajibade; ajibadep@ukzn.ac.za

Received 18 August 2018; Revised 1 November 2018; Accepted 5 November 2018; Published 2 January 2019

Academic Editor: Eduard Llobet

SnS nanocrystals were synthesized using bis(phenylpiperazine dithiocarbamate)tin(II) in oleic acid (OA) and octadecylamine (ODA) at three different temperatures (150, 190, and 230°C). XRD diffraction pattern confirms that OASnS and ODASnS nanoparticles are in the orthorhombic phase and the type of capping agent used affects the crystallinity. Transmission electron microscopy (TEM) images shows spherically shaped nanocrystals for oleic acid capped SnS (OASnS) while octadecylamine (ODASnS) are cubic. Monodispersed SnS of size range 10.67–17.74 nm was obtained at 150°C for OASnS while the biggest-sized nanocrystals were obtained at 230°C for ODASnS. Temperature and capping agents tuned the crystallite sizes and shapes of the as-prepared nanocrystals. Electron dispersive X-ray spectroscopy indicates the formation of tin sulphide with the presence of Sn and S peaks in the nanocrystals. Flowery and agglomerated spherical-like morphology were observed for ODASnS and OASnS nanocrystals, respectively, using a SEM (scanning electron microscope). Direct electronic band gaps of the synthesized SnS nanocrystals are 1.71–1.95 eV and 1.93–2.81 eV for OASnS and ODASnS nanocrystals, respectively.

1. Introduction

Tin is one of the relatively abundant metals having mild toxicity in comparison with other elements such as lead, mercury, and cadmium. Its rich structural chemistry is partly due to the +2 oxidation state which enable it to form compounds with different coordination geometries ranging from 2 to 9 [1–3]. SnS is a IV–VI semiconductor like PbS, PbSe, GeS, and SnS among others that exhibit size-dependent, luminescent, electrical, and optical properties [4–7]. Tin sulphide exists in three main forms: SnS, SnS_2, and SnS_3, with SnS having a band gap of 1.4 eV which is relatively close to that of silicon (1.1 eV) [8]. Tin sulphide exists as a orthorhombic crystal like distorted NaCl structure in which the Sn anion is surrounded by six S atoms separated by Van der Waals forces [2]. SnS nanoparticles have unique properties suitable for a wide range of nanoscale electronics, photodetectors, sensing devices, infrared detectors, storage of energy, and fabrication of photovoltaics [9–20]. SnS possesses photoconducting, photocatalytic, and Pieter effects making them useful in thermoelectric cooling, thermoelectric power generation, and near-infrared photoelectronics [16, 21–25].

Synthetic routes such as hydrothermal [26], solvothermal [27], hot injection [28], aqueous solution [29], pyrolysis [30], colloidal route [31], single-source approach [32, 33], precipitation [34], microwave [35], electrodeposition [36], and so on have been utilized for the synthesis of SnS nanoparticles. The single-source precursor has proven to be a more effective route that forms nanoparticles of high qualities with well-defined size and shape. The use of solvothermal decomposition of single-source precursors as capping agents at low temperatures resulted in high-quality SnS nanocrystals [37]. SnS usually form anisotropic nanostructure with various morphologies such as spherical or close to spherical [38], tetrahedral [39], nanocubes [40], triangular shape [41], nanorods [42], nanoflowers [43, 44], nanowires [36], nanoplatelets [45],and nanosheets [46]. Koktysh et al. [47] synthesized oleylamine-capped SnS nanoparticles from bis(diethyldithiocarbamato)tin(II) with

particle size in the range of 5–10 nm. It has been established that the control of nanoparticles morphology, size, and shape is influenced by the molecular precursor, the capping agents, and the reaction temperature [32, 48] which inherently affects the surface energy [49]. We report the effects of the capping agents and thermolysis temperature on the structural and optical properties of the as-prepared SnS nanoparticles from bis(phenylpiperazine dithiocarbamato) tin(II).

2. Experimental

2.1. Materials and Physical Measurements. *N*-phenyl piperazine, carbon disulphide, sodium hydroxide, tin(II) chloride dihydrate, trioctylphosphine, oleic acid, and octadecylamine of analytical grade were purchased from Sigma-Aldrich and used without further purifications. The FTIR of the ligand, complex and nanocrystals spectra were recorded using an Agilent technologies Cary 630 FTIR spectrometer in the frequency range of 4000–650 cm^{-1}. ^{1}H and ^{13}C-NMR of ligand and complex were recorded on an 400 MHz Bruker Avance III NMR spectrometer with tetramethylsilane serving as internal standard. Absorption spectra were obtained using an Agilent technologies Cary 100 UV-Vis spectrophotometer in the wavelength range of 200–800 nm. Photoluminescence emission was obtained using a PerkinElmer LS 45 fluorescence spectrometer. Melting point calculated using stuart SMP3 version 5.0. Transmission electron microscope (TEM) images of the nanocrystals were determined using a JEOL JEM-1400 transmission electron microscope with an accelerating voltage of 120 kV. The powder X-ray diffraction analysis was done using a Bruker D8 advanced diffractometer (Billerica, MA, USA). The morphology and compositions of tin sulphide nanocrystals were analysed using a Zeiss Evols 15 scanning electron microscope equipped with energy dispersive X-ray spectroscopy.

2.2. Synthesis of N-Phenyl Piperazine Dithiocarbamate Sn(II) Complex. Bis(phenylpiperazine dithiocarbamato)tin(II) was synthesized using modified literature procedures [33]. Briefly, 1.2 g (0.03 mol) of sodium hydroxide was dissolved in distilled water and allowed to cool in ice to which *N*-phenyl piperazine (4.58 mL, 0.03 mol) was added followed by cold carbon disulphide and allowed to stir in ice bath for 4 h. The product obtained (PhPipdtc) was filtered and washed using diethyl ether and allowed to dry. The dried sodium *N*-phenyl piperazine dithiocarbamate (PhPipdtc) was then dissolved in 50 mL of methanol, and 0.015 mol of tin(II) chloride dihydrate dissolved in 25 mL of methanol was added dropwise to the dithiocarbamate methanolic solution and stirred at room temperature for 3 hours (Scheme 1). The resulting precipitate was washed with water then followed by diethyl ether. The complex $[Sn(PhPipdtc)_2]$ obtained was orange in colour. Yield: 83.99%, 1.9897 g; melting point: 212.4–214.9°C. **PhPipdtc**: anal. cal. for $C_{11}H_{13}N_2NaS_2{\cdot}H_2O$: C, 44.58; H, 5.78; N, 9.45; found: C, 44.22; H, 5.65; N, 9.16. ESIMS (*m/z*): 237 $[M\text{-}Na]^-$, selected IR bands (cm^{-1}): 1006 (CS_2), 1462 (N-CS_2). ^{1}H-NMR: (D_2O) δ 3.23 (t, 4H–CH_2), 4.50 (t, 4H–CH_2), 7.07–7.41 (m, 5H-C_6H_5); ^{13}C-NMR: (D_2O) δ 49.70–50.45 (C_4N_2), 117.98–150.33 (C_6H_5), 209.0 (CS_2). **[Sn(PhPipdtc)$_2$]**: anal. cal. for $C_{22}H_{28}N_4NaS_4Sn$: C, 44.38; H, 4.74; N, 9.41; found: C, 44.54; H, 5.01; N, 9.09. ESIMS (*m/z*): 618 $[M\text{-}Na]^+$, selected IR bands (cm^{-1}): 915 (CS_2), 1489 (N-CS_2). ^{1}H-NMR: (DMSO) δ 3.18 (t, 4H–CH_2), 3.31 (t, 4H–CH_2), 6.88–7.27 (m, 5H-C_6H_5); ^{13}C-NMR: (DMSO) δ 43.70–47.2 (C_4N_2), 116.4–150.94 (C_6H_5), 204.3 (CS_2).

2.3. Synthesis of SnS Nanocrystals. 0.2 g of Sn(II) phenyl piperazine dithiocarbamate complex was dispersed in 1 mL trioctylphosphine (TOP). The resulting solution was injected into hot 4 g of octadecylamine in a three-necked round bottom flask at 150, 190, and 230°C. There was a reduction in temperature of about 12–25°C, after which it was allowed to stabilize at the desired temperature and then stirred for 1 hour. The reaction was left to cool to 70°C followed by the addition of cold methanol. The flocculate was then centrifuged at 3500 rpm for 30 minutes, and the supernatant was decanted and washed severally. The nanocrystals were dispersed in hexane for further analysis. The same procedure was repeated using 6 mL of oleic acid. The resulting nanocrystals prepared from octadecylamine were labelled ODASn1 (150°C), ODASn2 (190°C), and ODASn3 (230°C). Those prepared from oleic acid were labelled OASnS1 (150°C), OASnS2 (190°C), and OASnS3 (230°C).

3. Results and Discussion

3.1. Spectroscopic Studies of PhPipdtc and [Sn(PhPipdtc)$_2$]. The phenyl-piperazine dithiocarbamate (Phpipdtc) electronic spectrum exhibited three absorption bands attributed to $\pi \longrightarrow \pi^*$ of υ|N–C=S| at 252 nm, $\pi \longrightarrow \pi^*$ of υ|C–S=S| at 277 nm, and $n \longrightarrow \pi^*$ of the sulphur atoms at 337 nm [50]. On complexation, the absorption band of υ|C=N| chromophore was observed at 265 nm due to the thioureide group intramolecular transition in the Sn(II) dithiocarbamate complex [51]. The υ|N–CS_2| band observed at 1462 cm^{-1} in the ligand spectrum shifted to 1489 cm^{-1} in the complex due to the delocalization of the electron from the nitrogen attached to the thioureide moiety confirming the coordination of tin(II) ion to the ligand [52]. The ν|C–S| symmetrical vibrational band peak observed in the ligand at 994 cm^{-1} as two peaks shifted to 915 cm^{-1} as a single peak on coordination to tin(II) ion. It has been established that a single band around 1000 ± 70 cm^{-1} in metal dithiocarbamate complexes is attributed to bidentate coordination of the dithiocarbamate moiety while the splitting of the band in this region indicates the monodentate coordination mode [53]. The ^{1}H-NMR spectrum of PhPipdtc showed the methylene proton of piperazine signals at 3.23 ppm and 4.50 ppm as triplet. The downfield resonance at 4.50 ppm is because of the thioureide nitrogen while the phenyl proton resonated at a higher frequency of 7.07–7.41 ppm. On complexation, phenyl protons shifted to 6.88–7.27 ppm, while the methylene protons resonated at 3.18

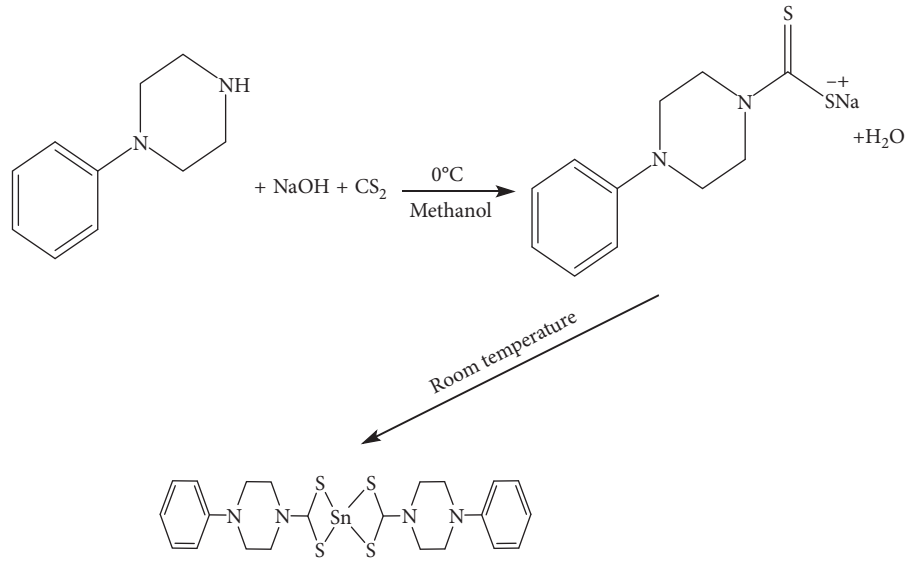

Scheme 1: Synthesis of bis(phenylpiperazine dithiocarbamato)tin(II).

and 3.31 ppm. The desheilding effect is due to delocalization of thioureide nitrogen towards the sulphur atoms which increases electronegativity of the surrounding protons [54]. The ^{13}C-NMR spectrum shows the piperazine carbon resonating at 49.70–50.45 ppm, and the phenyl carbons resonating at 117.98–150.33 ppm with the thioureide carbon resonating at 209.0 ppm. On complexation, the piperazine carbon shifted upfield to 43.7–47.2 ppm, while the phenyl carbons have a desheilding resonance at 116.4–150.94 ppm. The thioureide carbon shifted to 204.3 ppm because of the coordination of tin(II) ion to the thioureide sulphur.

3.2. Structural Studies of SnS Nanocrystals

3.2.1. X-Ray Diffraction of SnS Nanocrystals. The XRD patterns of oleic acid capped tin sulphide nanoparticles (Figure 1(a)) show four well-defined peaks at 30.90°, 34.73°, 39.37°, and 60.36° corresponding to (111), (101), (131), and (201) planes of orthorhombic crystal structure of SnS. The preferred orientation along the (111) plane was observed correlating with the standard values of JCPD card no 39–0354 [55]. The relatively smaller broad diffraction peaks suggest smaller particle sizes. Sharp intense peaks in the XRD patterns of ODASnS (Figure 1(b)) at 22.37°, 24.78°, 25.45°, 27.54°, 33.65°, 41.90°, and 47.27° correspond to (110), (110), (120), (120), (111), (311), and (002) of SnS which is similar to Pullabholla and Maliba [56] observation using HDA (hexadecylamine) as a capping agent. The sharp and narrow peaks of (120) and (101) with high intensity show that the nanoparticles are purely SnS which is also of orthorhombic phase. The difference in the XRD pattern is due to the different capping agents used.

3.2.2. Transmission Electron Microscopic Analysis of SnS Nanocrystals. TEM images of SnS nanocrystals showed spherical and cubic shapes as presented in Figure 2. The as-synthesized SnS nanocrystals show diverse size and shape by varying the temperature and capping agents. OASnS nanocrystals has monodispersed spherical shape with different sizes at various temperatures such as 10.67–28.74 nm, 12.82–17.10 nm, and 35.25–75.10 nm, respectively, for 150, 190, and 230°C showing that temperature influences the sizes of the nanocrystals obtained. ODASnS nanocrystals are spherical shaped of size range 22.00–28.32 nm at 150°C, which changed to agglomerated nanocrystals cubes at 190°C with particle size in the range of 28.15–33.36 nm. At 230°C, there was increase in size to 67.04–80.15 nm while maintaining the cubic shape. Agglomeration was observed to increase as the temperature increases this could be due to surface attraction of the nanocrystals. OA and ODA capped SnS nanocrystals followed the trend of increase in size with increase in temperature. The capping agents used showed various degrees of sizes. Oleic acid gave smaller size SnS nanocrystals of monodispersed spherical shape, while octadecylamine has bigger agglomerated nanocrystals with cube-like shape.

3.2.3. SEM Analysis and EDX Spectra of SnS Nanocrystals. The influence of capping agents and reaction temperature on the SnS nanoparticle morphology was investigated using SEM as shown in Figure 3. OASnS nanocrystals had spherical aggregates. The morphologies of ODASnS were different from those of OASnS as they showed flaky-like morphology [57]. The SEM images show diversity in morphology due to different capping agents used in the preparation of tin sulphide. Temperature has no effect on the morphology of OASnS and ODASnS. Carbon and oxygen signals were observed in the EDX (electron dispersive X-ray) spectra (Figure 4) of SnS nanocrystals; this is because of the capping agents used and the carbon tape. The presence of Sn and S peaks is an indication that SnS nanocrystals were

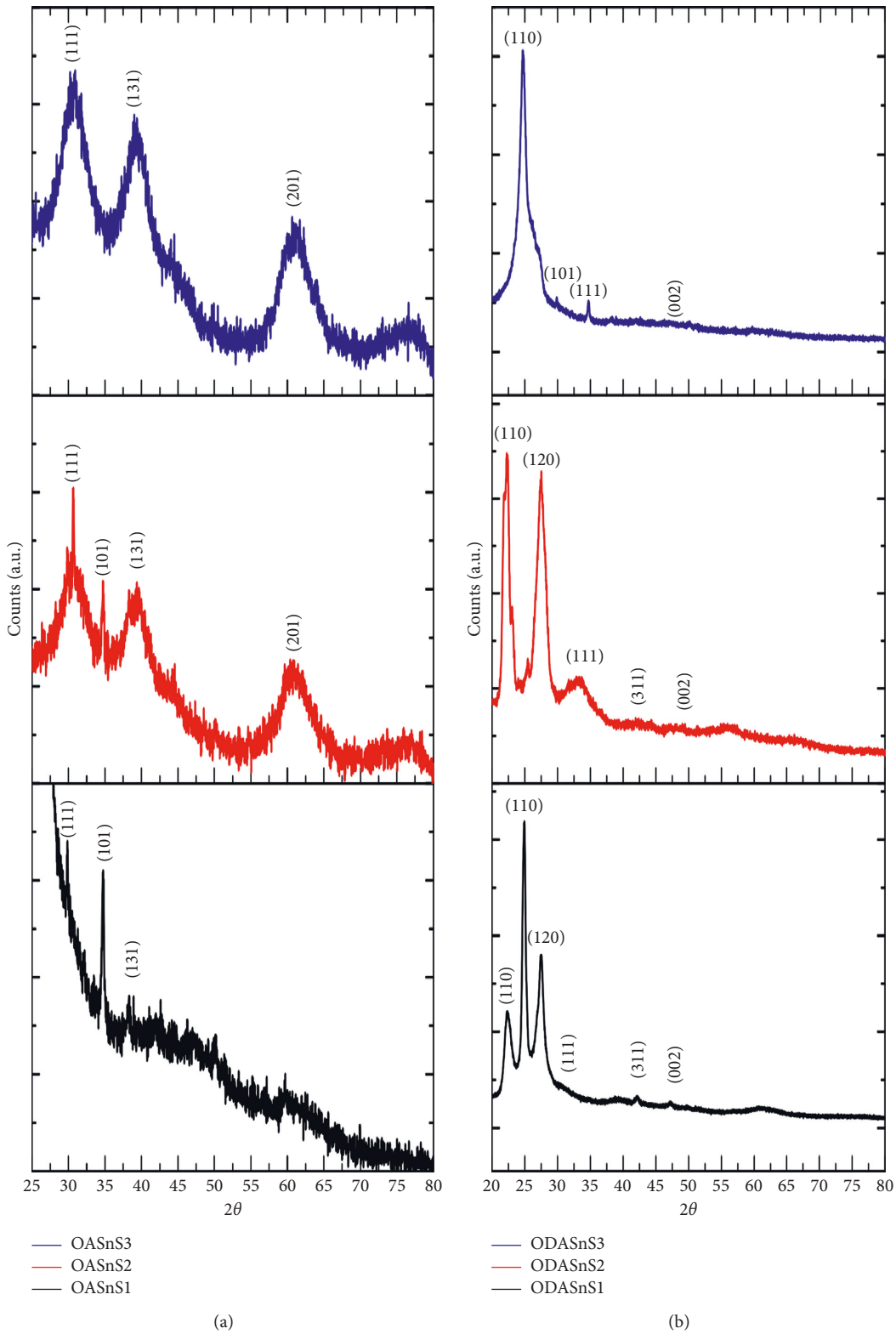

Figure 1: XRD diffraction pattern of OASnS (a) and ODASnS (b).

formed. OA-capped SnS showed elemental composition of 53% to 47% of Sn and S at all temperatures, and ODASnS nanocrystals composition was 52% to 48%. The presence of excess sulphur is an indication of dangling sulphur bonds. In all the SnS nanocrystals of various capping agents, the composition of Sn is slightly more than S, while a change in temperature has no effect on the composition of SnS nanocrystals showing its stability [58].

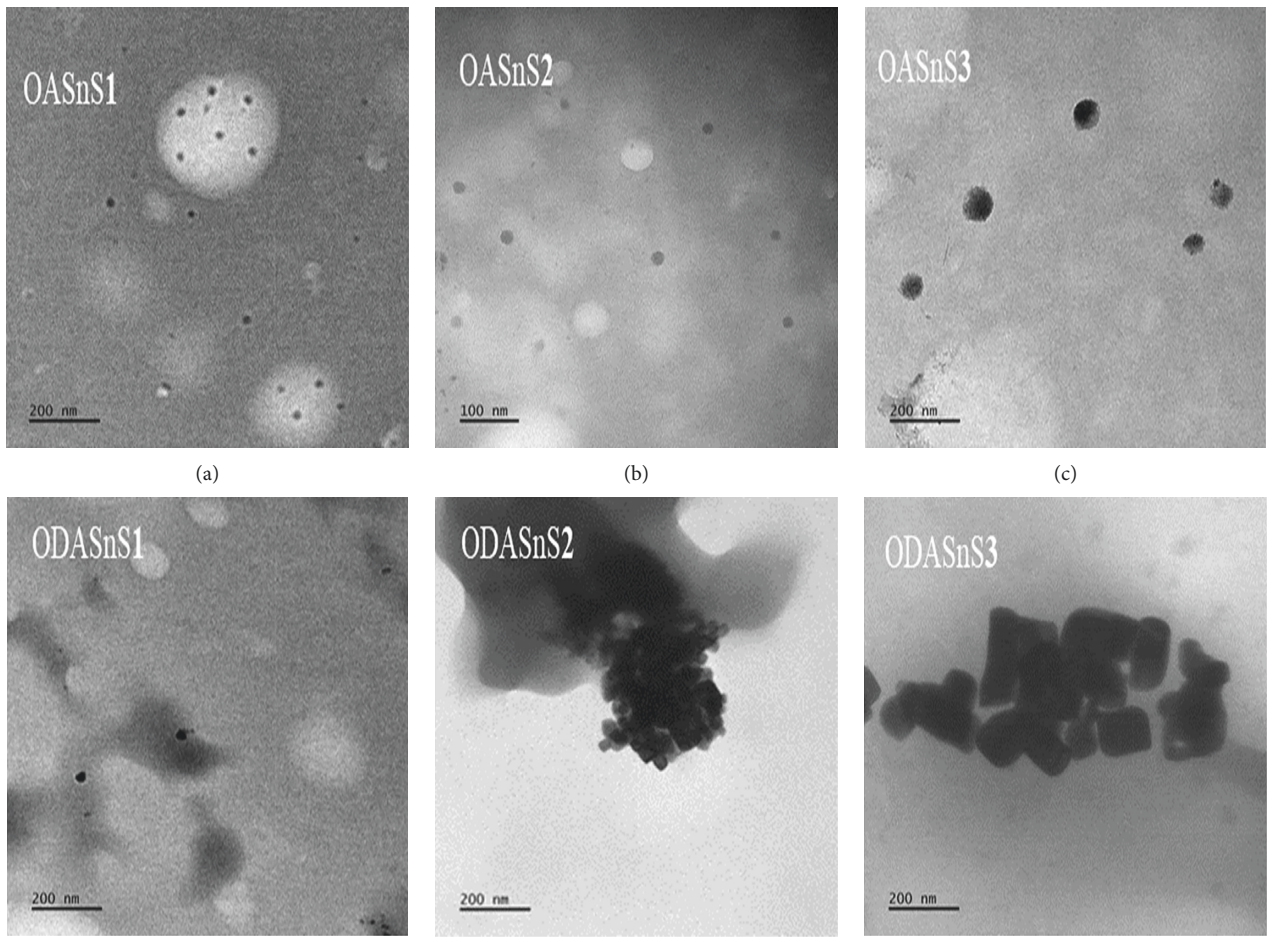

(a) (b) (c)

(d) (e) (f)

Figure 2: TEM images of OASnS1 (a), OASnS2 (b), and OASnS3 (c). TEM images of ODASnS1 (d), ODASnS2 (e), and ODASnS3 (f).

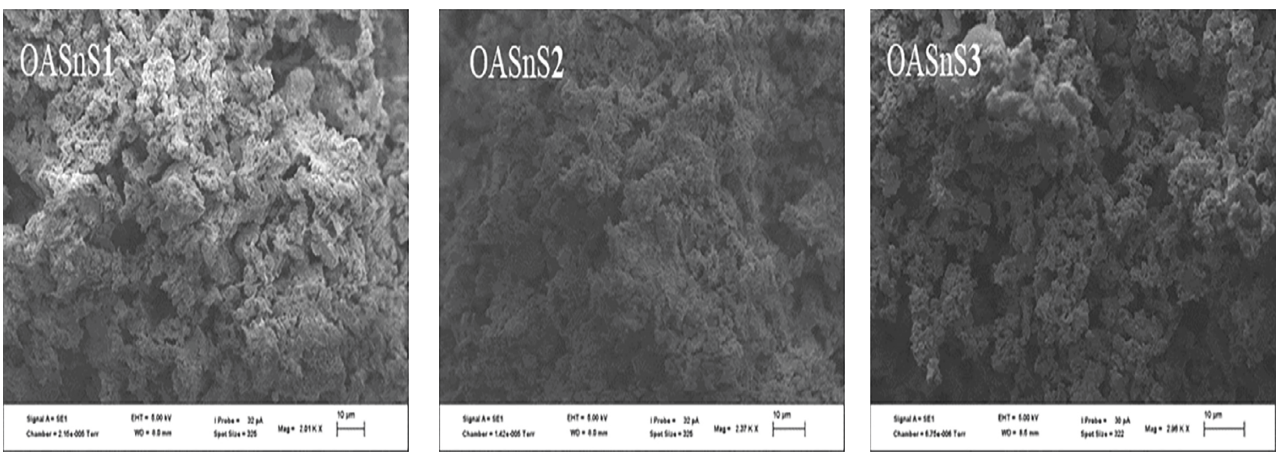

(a) (b) (c)

Figure 3: Continued.

(d) (e) (f)

Figure 3: SEM images of OASnS1 (a), OASnS2 (b), and OASnS3 (c). SEM images of ODASnS1 (d), ODASnS2 (e), and ODASnS3 (f).

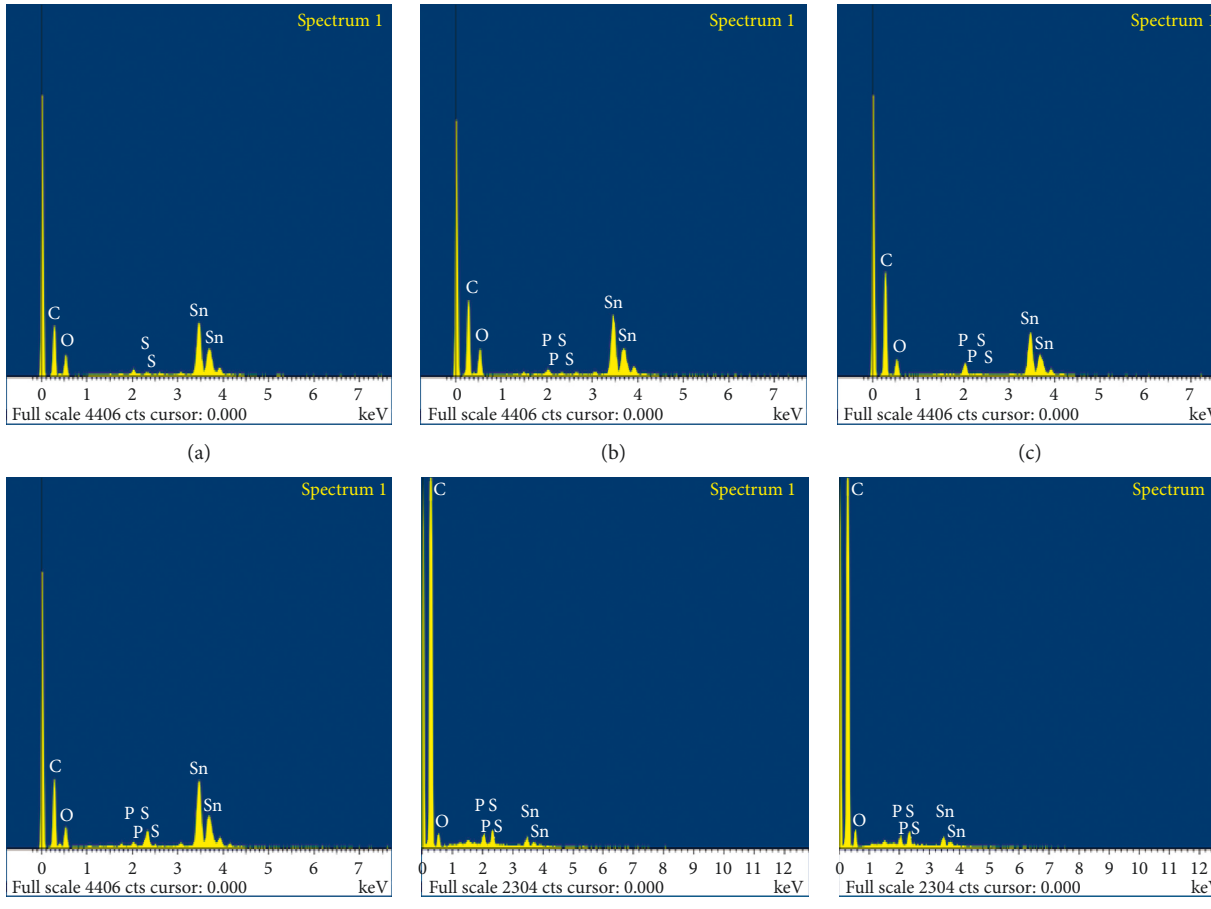

(a) (b) (c)

(d) (e) (f)

Figure 4: EDX spectra of OASnS1 (a), OASnS2 (b), OASnS3 (c), ODASnS1 (d), ODASnS2 (e), and ODASnS3 (f).

3.4. Optical Studies of SnS Nanocrystals. Quantum confinement makes semiconductors' nanoscale band gap deviate from their bulk band gap, and this is caused by photogenerated electron-hole pairs [40, 59]. To obtain the band gap of the synthesized SnS nanocrystals, the absorption spectra data were measured in the wavelength range of 300–800 nm at room temperature. Tauc's analysis was used for conversion by utilizing the near-edge absorption equation $(\alpha h\nu)^n = A(h\nu - Eg)$, where α is the wavelength-dependent absorption coefficient, A is a constant, $h\nu$ is

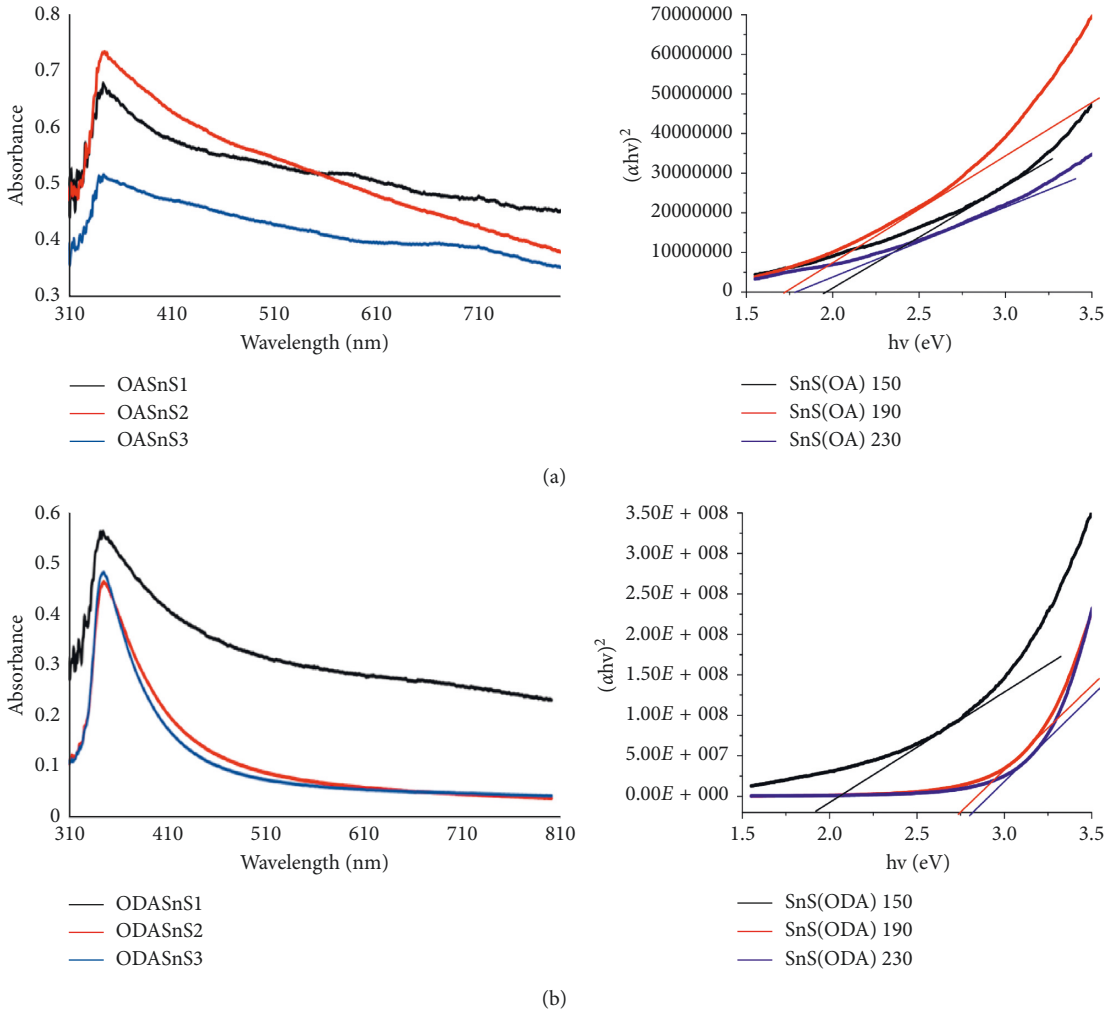

Figure 5: UV-Vis absorption spectra of OASnS with its Tauc plot (a) and ODASnS with its Tauc plot (b).

the photon energy, and *Eg* is the band gap. The transition process was denoted as "n" which can be 1/2 for indirect allowed transitions, 1/3 for indirect forbidden transition, 2/3 for direct forbidden transition, and 2 for direct allowed transition. In this study, the direct allowed transition was used as a good fit of extrapolation was obtained by plotting $(\alpha hv)^2$ against hv and extrapolating the x-axis value [33, 60]. The band gap is in the range of 1.71–1.95 eV for OASnS and 1.93–2.81 eV for ODASnS nanocrystals (Figure 5) which is higher than 1.4 eV of bulk SnS [61] exhibiting blue shift of the band gap. SnS band gap for direct allowed transitions of 1.0–1.7 eV has been reported [62–64]. Increase in the band gap of the SnS nanoparticle could be attributed to combination of strain, particle size confinement, and defects and disorder of grain boundaries [33, 65]. The capping agents and temperature influence the band gap; the highest band gap energy (2.81 eV) was obtained at 230°C for ODASnS nanoparticle. The UV-Vis absorption spectra presented in Figure 5 show the nanocrystals having absorption at 337 nm for OASnS1 and 345 nm for ODASnS1 while those of the remaining nanocrystals occurred at 348 nm. Wavelength band shows quantum confinement effect as lower wavelength implies smaller diameter and vice versa [59, 66]. The photoluminescence spectra of SnS nanocrystals were recorded at room temperature at an excitation wavelength of 350 nm (Figures 6–7); strong and broad emission peaks maximum was obtained at 408–431 nm for ODASnS while OASnS has a sharp emission band [51, 67].

3.5. FTIR Studies of SnS Nanocrytals. The FTIR spectra of OASnS and ODASnS nanocrystals were compared with their respective capping agents for the confirmation of their coating (Figure 8). NH_2 bending modes were observed at 927–966 and 1058–1070 cm^{-1} in ODASnS nanocrystals which were present at 964 cm^{-1} in the capping agents alongside the N-H wagging mode at 793 cm^{-1} which is absent in the nanocrystal spectra. This can be attributed to the inhibition of the wagging mode due to its attachment to the surface of SnS as reported in literature [68–70]. C-N bending vibrations were observed at 1468 cm^{-1}, and the combination of NH_2 scissor and bending vibration at 1668 cm^{-1} in the capping agents and their nanocrystals. The difference observed is that the nanocrystals has less intensity compared to the capping agents, and a shift of 20–60 cm^{-1} was observed for the NH_2 scissors and bending vibrations.

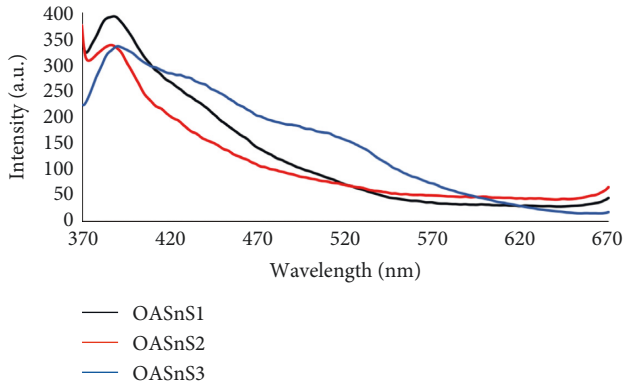

Figure 6: Photoluminescence spectra of OASnS.

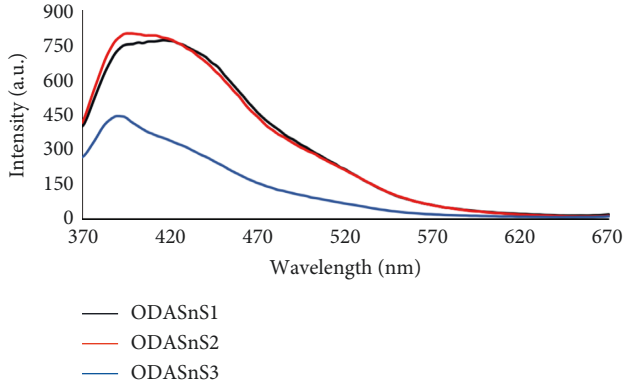

Figure 7: Photoluminescence spectra of ODASnS.

The N-H asymmetric peak observed at 3329 cm^{-1} is weak in the nanocrystals confirming interaction between the amine and the SnS surface [71]. C-H vibrations were found at 2851–2919 cm^{-1} which is common to $(CH_2)_n$ chains more than 3. Carbonyl vibration, deformed vibration, and rocking vibration of CH_2 were observed, respectively, at 1710, 1465, and 722 cm^{-} in OASnS nanocrystals apart from the carbonyl bond which disappeared and a new band at 1599–1606 cm^{-1} appeared which is the asymmetric mode of carboxylate metal salt [68, 72, 73].

4. Conclusion

In conclusion, we report the synthesis and use of bis(phenylpiperazine dithiocarbamate)tin(II) complex as a single molecular precursor to prepare oleic acid and octadecylamine capped at 150, 190, and 230°C. The crystallinity of the synthesized tin sulphide nanoparticles was affected by the capping agents used though the same orthorhombic phase was observed with the XRD pattern. Monodispersed spherical-shaped SnS nanoparticles were obtained in OASnS, while ODASnS nanocrystals gave aggregated cubic nanocrystals. At 150°C, small-sized nanocrystals in the range of 10–28 nm were favoured in all the capping agents, while at 230°C, bigger size in the range of 35–80 nm was obtained. The morphology was

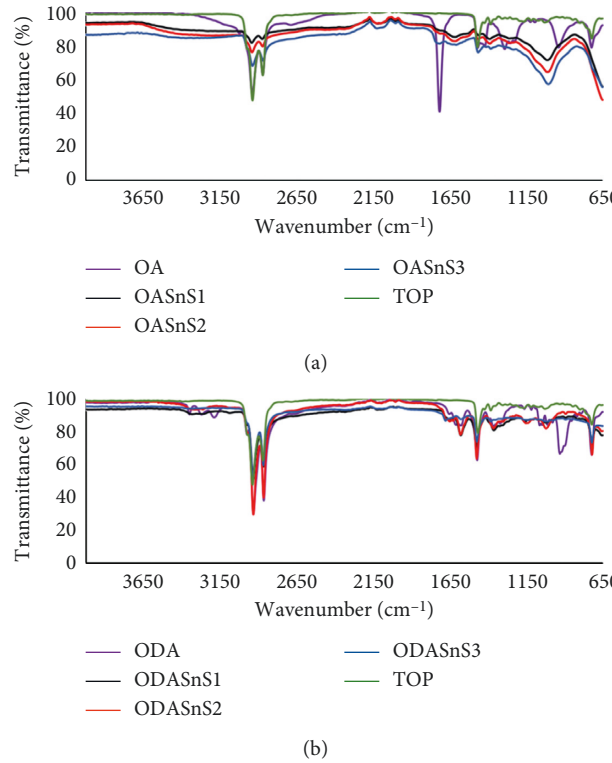

Figure 8: FTIR spectra overlay of OASnS nanocrystals (a) and ODASnS nanocrystals (b).

influenced by the capping agents used as flower-like, and spherical-like morphologies were obtained for ODASnS and OASnS nanocrystals. Band gap measurements were in the range of 1.71–1.95 and 1.93–2.81 eV for OASnS and ODASnS, respectively; the highest band gap is affected by particle size confinement. Temperature and capping agents were found to influence the size and shape of the nanocrystals. SnS FTIR showed that they were coated with the capping agents.

Data Availability

The data used to support the findings of this study are available from the authors upon request.

Conflicts of Interest

The authors declare that there are no conflicts of interest.

Authors' Contributions

AE Oluwalana carried out the experimental in the laboratory of PA Ajibade and under his guidance.

Acknowledgments

The authors acknowledge the award of research grant by the National Research Foundation and Sasol, South Africa.

References

[1] P. D. Antunez, J. J. Buckley, and R. L. Brutchey, "Tin and germanium monochalcogenide IV–VI semiconductor nanocrystals for use in solar cells," *Nanoscale*, vol. 3, no. 6, pp. 2399–2411, 2011.

[2] T. Jiang and G. A. Ozin, "New directions in tin sulfide materials chemistry," *Journal of Materials Chemistry*, vol. 8, no. 5, pp. 1099–1108, 1998.

[3] P. Sinsermsuksakul, L. Sun, S. W. Lee et al., "Overcoming efficiency limitations of SnS-based solar cells," *Advanced Energy Materials*, vol. 4, no. 15, article 1400496, 2014.

[4] N. C. Anderson, M. P. Hendricks, J. J. Choi, and J. S. Owen, "Ligand exchange and the stoichiometry of metal chalcogenide nanocrystals: spectroscopic observation of facile metal-carboxylate displacement and binding," *Journal of the American Chemical Society*, vol. 135, no. 49, pp. 18536–18548, 2013.

[5] D. Zherebetskyy, M. Scheele, Y. Zhang et al., "Hydroxylation of the surface of PbS nanocrystals passivated with oleic acid," *Science*, vol. 344, no. 6190, pp. 1380–1384, 2014.

[6] O. E. Semonin, J. C. Johnson, J. M. Luther, A. G. Midgett, A. J. Nozik, and M. C. Beard, "Absolute photoluminescence quantum yields of IR-26 dye, PbS, and PbSe quantum dots," *The Journal of Physical Chemistry Letters*, vol. 1, no. 16, pp. 2445–2450, 2010.

[7] A. D. Antu, Z. Jiang, S. M. Premathilka et al., "Bright colloidal PbS nanoribbons," *Chemistry of Materials*, vol. 30, no. 11, pp. 3697–3703, 2018.

[8] D. J. Lewis, P. Kevin, O. Bakr, C. A. Muryn, M. A. Malik, and P. O'Brien, "Routes to tin chalcogenide materials as thin films or nanoparticles: a potentially important class of semiconductor for sustainable solar energy conversion," *Inorganic Chemistry Frontiers*, vol. 1, no. 8, pp. 577–598, 2014.

[9] D. V. Talapin, J.-S. Lee, M. V. Kovalenko, and E. V. Shevchenko, "Prospects of colloidal nanocrystals for electronic and optoelectronic applications," *Chemical Reviews*, vol. 110, no. 1, pp. 389–458, 2009.

[10] D. V. Kosynkin, W. Lu, A. Sinitskii, G. Pera, Z. Sun, and J. M. Tour, "Highly conductive graphene nanoribbons by longitudinal splitting of carbon nanotubes using potassium vapor," *ACS Nano*, vol. 5, no. 2, pp. 968–974, 2011.

[11] C. Kim, J. C. Park, S. Y. Choi et al., "Self-Formed channel devices based on vertically grown 2D materials with large-surface-area and their potential for chemical sensor applications," *Small*, vol. 14, no. 15, article 1704116, 2018.

[12] R. Li, K. Jiang, S. Chen et al., "SnO_2/SnS_2 nanotubes for flexible room-temperature NH 3 gas sensors," *RSC Advances*, vol. 7, no. 83, pp. 52503–52509, 2017.

[13] I.-H. Baek, J. J. Pyeon, Y. G. Song et al., "Synthesis of SnS thin films by atomic layer deposition at low temperatures," *Chemistry of Materials*, vol. 29, no. 19, pp. 8100–8110, 2017.

[14] Z. Zhang, J. Yang, K. Zhang, S. Chen, F. Mei, and G. Shen, "Anisotropic photoresponse of layered 2D SnS-based near infrared photodetectors," *Journal of Materials Chemistry C*, vol. 5, no. 43, pp. 11288–11293, 2017.

[15] M. Kumar, M. Patel, J. Kim, and D. Lim, "Enhanced broadband photoresponse of a self-powered photodetector based on vertically grown SnS layers via the pyro-phototronic effect," *Nanoscale*, vol. 9, no. 48, pp. 19201–19208, 2017.

[16] B. Luo, J. Zhao, B. Cheng et al., "A surface state-controlled, high-performance, self-powered photovoltaic detector based on an individual SnS nanorod with a symmetrical electrode structure," *Journal of Materials Chemistry C*, vol. 6, no. 34, pp. 9071–9080, 2018.

[17] Y. Fu, G. Gou, X. Wang et al., "High-performance photodetectors based on CVD-grown high-quality SnS_2 nanosheets," *Applied Physics A*, vol. 123, no. 4, pp. 299–306, 2017.

[18] P. He, Y. Fang, X. Y. Yu, and X. W. Lou, "Hierarchical nanotubes constructed by carbon-coated ultrathin SnS nanosheets for fast capacitive sodium storage," *Angewandte Chemie*, vol. 129, no. 40, pp. 12370–12373, 2017.

[19] B. Zhao, F. Chen, Z. Wang, S. Huang, Y. Jiang, and Z. Chen, "Lithiation-assisted exfoliation and reduction of SnS_2 to SnS decorated on lithium-integrated graphene for efficient energy storage," *Nanoscale*, vol. 9, no. 45, pp. 17922–17932, 2017.

[20] H. Ye, H. Li, F. Jiang, J. Yin, and H. Zhu, "In situ fabrication of nitrogen-doped carbon-coated SnO2/SnS heterostructures with enhanced performance for lithium storage," *Electrochimica Acta*, vol. 266, pp. 170–177, 2018.

[21] Y. Hu, T. Chen, X. Wang et al., "Controlled growth and photoconductive properties of hexagonal SnS_2 nanoflakes with mesa-shaped atomic steps," *Nano Research*, vol. 10, no. 4, pp. 1434–1447, 2017.

[22] I. Shown, S. Samireddi, Y.-C. Chang et al., "Carbon-doped SnS 2 nanostructure as a high-efficiency solar fuel catalyst under visible light," *Nature communications*, vol. 9, no. 1, pp. 169–178, 2018.

[23] Z. Deng, D. Cao, J. He, S. Lin, S. M. Lindsay, and Y. Liu, "Solution synthesis of ultrathin single-crystalline SnS nanoribbons for photodetectors via phase transition and surface processing," *ACS Nano*, vol. 6, no. 7, pp. 6197–6207, 2012.

[24] A. Chen, S. Xia, X. Pan, H. Lu, and Z. Ji, "Easily removable visible-light-driven photocatalyst of nickel modified SnS2 nanosheets for reduction of Cr (VI)," *Journal of Alloys and Compounds*, vol. 735, pp. 1314–1318, 2018.

[25] F. Jamali-Sheini, M. Cheraghizade, and R. Yousefi, "Ultrasonic synthesis of In-doped SnS nanoparticles and their physical properties," *Solid State Sciences*, vol. 79, pp. 30–37, 2018.

[26] K. Manukumar, G. Nagaraju, B. Kishore, C. Madhu, and N. Munichandraiah, "Ionic liquid-assisted hydrothermal synthesis of SnS nanoparticles: electrode materials for lithium batteries, photoluminescence and photocatalytic activities," *Journal of energy chemistry*, vol. 27, no. 3, pp. 806–812, 2018.

[27] H. Chauhan, M. K. Singh, S. Hashmi, and S. Deka, "Synthesis of surfactant-free SnS nanorods by a solvothermal route with better electrochemical properties towards supercapacitor applications," *RSC Advances*, vol. 5, no. 22, pp. 17228–17235, 2015.

[28] P.-C. Huang, H.-I. Wang, S. Brahma, S.-C. Wang, and J.-L. Huang, "Synthesis and characteristics of layered SnS2 nanostructures via hot injection method," *Journal of Crystal Growth*, vol. 468, pp. 162–168, 2017.

[29] P. Nørby, S. Johnsen, and B. B. Iversen, "Fine tunable aqueous solution synthesis of textured flexible SnS 2 thin films and nanosheets," *Physical Chemistry Chemical Physics*, vol. 17, no. 14, pp. 9282–9287, 2015.

[30] X. Dai, C. Shi, Y. Zhang, F. Liu, X. Fang, and J. Zhu, "SnS thin film prepared by pyrolytic synthesis as an efficient counter electrode in quantum dot sensitized solar cells," *Journal of nanoscience and nanotechnology*, vol. 15, no. 9, pp. 6813–6817, 2015.

[31] D. Yin, Y. Liu, C. Dun, D. L. Carroll, and M. T. Swihart, "Controllable colloidal synthesis of anisotropic tin dichalcogenide nanocrystals for thin film thermoelectrics," *Nanoscale*, vol. 10, no. 5, pp. 2533–2541, 2018.

[32] J. R. Thompson, I. Y. Ahmet, A. L. Johnson, and G. Kociok-Köhn, "Tin (IV) chalcogenide complexes: single source

precursors for SnS, SnSe and SnTe nanoparticle synthesis," *European Journal of Inorganic Chemistry*, vol. 2016, no. 28, pp. 4711–4720, 2016.

[33] P. Kevin, D. J. Lewis, J. Raftery, M. A. Malik, and P. O'Brien, "Thin films of tin (II) sulphide (SnS) by aerosol-assisted chemical vapour deposition (AACVD) using tin (II) dithiocarbamates as single-source precursors," *Journal of Crystal Growth*, vol. 415, pp. 93–99, 2015.

[34] J. Henry, K. Mohanraj, S. Kannan, S. Barathan, and G. Sivakumar, "Structural and optical properties of SnS nanoparticles and electron-beam-evaporated SnS thin films," *Journal of Experimental Nanoscience*, vol. 10, no. 2, pp. 78–85, 2015.

[35] S. Park, J. Park, R. Selvaraj, and Y. Kim, "Facile microwave-assisted synthesis of SnS_2 nanoparticles for visible-light responsive photocatalyst," *Journal of Industrial and Engineering Chemistry*, vol. 31, pp. 269–275, 2015.

[36] Y.-T. Lin, J.-B. Shi, Y.-C. Chen, C.-J. Chen, and P.-F. Wu, "Synthesis and characterization of tin disulfide (SnS_2) nanowires," *Nanoscale Research Letters*, vol. 4, no. 7, pp. 694–698, 2009.

[37] N. Pradhan, B. Katz, and S. Efrima, "Synthesis of high-quality metal sulfide nanoparticles from alkyl xanthate single precursors in alkylamine solvents," *The Journal of Physical Chemistry B*, vol. 107, no. 50, pp. 13843–13854, 2003.

[38] A. de Kergommeaux, J. R. M. Faure-Vincent, A. Pron, R. M. de Bettignies, B. Malaman, and P. Reiss, "Surface oxidation of tin chalcogenide nanocrystals revealed by 119Sn–Mössbauer spectroscopy," *Journal of the American Chemical Society*, vol. 134, no. 28, pp. 11659–11666, 2012.

[39] B. K. Patra, S. Sarkar, A. K. Guria, and N. Pradhan, "Monodisperse SnS nanocrystals: in just 5 seconds," *Journal of Physical Chemistry Letters*, vol. 4, no. 22, pp. 3929–3934, 2013.

[40] A. J. Biacchi, D. D. Vaughn, and R. E. Schaak, "Synthesis and crystallographic analysis of shape-controlled SnS nanocrystal photocatalysts: evidence for a pseudotetragonal structural modification," *Journal of the American Chemical Society*, vol. 135, no. 31, pp. 11634–11644, 2013.

[41] C. W. S. G. Hickey, B. Rellinghaus, and E. Alexander, "Size and shape control of colloidally synthesized IV-VI nanoparticulate tin(II) sulfide," *Journal of America Chemical Society*, vol. 130, no. 45, pp. 14978–14980, 2008.

[42] A. M. Tripathi and S. Mitra, "Tin sulfide (SnS) nanorods: structural, optical and lithium storage property study," *RSC Advances*, vol. 4, no. 20, pp. 10358–10366, 2014.

[43] A. Patil, A. Lokhande, P. Shinde, H. Shelke, and C. Lokhande, "Electrochemical supercapacitor properties of SnS thin films deposited by low-cost chemical bath deposition route," *International Journal of Engineering Science*, vol. 10, pp. 914–922, 2017.

[44] J. Ning, K. Men, G. Xiao et al., "Facile synthesis of IV–VI SnS nanocrystals with shape and size control: nanoparticles, nanoflowers and amorphous nanosheets," *Nanoscale*, vol. 2, no. 9, pp. 1699–1703, 2010.

[45] A. de Kergommeaux, M. Lopez-Haro, S. Pouget et al., "Synthesis, internal structure, and formation mechanism of monodisperse tin sulfide nanoplatelets," *Journal of the American Chemical Society*, vol. 137, no. 31, pp. 9943–9952, 2015.

[46] Y. Zhang, J. Lu, S. Shen, H. Xu, and Q. Wang, "Ultralarge single crystal SnS rectangular nanosheets," *Chemical Communications*, vol. 47, no. 18, pp. 5226–5228, 2011.

[47] D. S. Koktysh, J. R. McBride, and S. J. Rosenthal, "Synthesis of SnS nanocrystals by the solvothermal decomposition of a single source precursor," *Nanoscale Research Letters*, vol. 2, no. 3, pp. 144–148, 2007.

[48] M. Yarema, R. Caputo, and M. V. Kovalenko, "Precision synthesis of colloidal inorganic nanocrystals using metal and metalloid amides," *Nanoscale*, vol. 5, no. 18, pp. 8398–8410, 2013.

[49] T. Mirkovic, M. A. Hines, P. S. Nair, and G. D. Scholes, "Single-source precursor route for the synthesis of EuS nanocrystals," *Chemistry of Materials*, vol. 17, no. 13, pp. 3451–3456, 2005.

[50] A. M. Paca and P. A. Ajibade, "Synthesis and structural studies of iron sulphide nanocomposites prepared from Fe (III) dithiocarbamates single source precursors," *Materials Chemistry and Physics*, vol. 202, pp. 143–150, 2017.

[51] T. Chintso and P. A. Ajibade, "Synthesis and structural studies of hexadecylamine capped lead sulfide nanoparticles from dithiocarbamate complexes single source precursors," *Materials Letters*, vol. 141, pp. 1–6, 2015.

[52] L. Ronconi, L. Giovagnini, C. Marzano et al., "Gold dithiocarbamate derivatives as potential antineoplastic agents: design, spectroscopic properties, and in vitro antitumor activity," *Inorganic Chemistry*, vol. 44, no. 6, pp. 1867–1881, 2005.

[53] N. H. Abdullah, Z. Zainal, S. Silong, M. I. M. Tahir, K.-B. Tan, and S.-K. Chang, "Synthesis of zinc sulphide nanoparticles from thermal decomposition of zinc N-ethyl cyclohexyl dithiocarbamate complex," *Materials Chemistry and Physics*, vol. 173, pp. 33–41, 2016.

[54] F. P. Andrew and P. A. Ajibade, "Synthesis, characterization and anticancer studies of bis (1-phenylpiperazine dithiocarbamato) Cu (II), Zn (II) and Pt (II) complexes: crystal structures of 1-phenylpiperazine dithiocarbamato-S, S′ zinc (II) and Pt (II)," *Journal of Molecular Structure*, vol. 1170, pp. 24–29, 2018.

[55] S. Rahaman, K. Jagannatha, A. Sriram, Anirudha, and Nitin, "Synthesis and characterization of SnS quantum dots materialfor solar cell," *Materials Today: Proceedings*, vol. 5, no. 1, pp. 3117–3120, 2018.

[56] V. R. Pullabhotla and M. Mabila, "A simple single molecular precursor route in the synthesis of high quality SnS nanoparticles," *Materials Letters*, vol. 183, pp. 30–33, 2016.

[57] X. Yan, E. Michael, S. Komarneni, J. R. Brownson, and Z.-F. Yan, "Microwave-and conventional-hydrothermal synthesis of CuS, SnS and ZnS: optical properties," *Ceramics International*, vol. 39, no. 5, pp. 4757–4763, 2013.

[58] C. Gurnani, S. L. Hawken, A. L. Hector et al., "Tin (iv) chalcogenoether complexes as single source precursors for the chemical vapour deposition of SnE_2 and SnE (E = S, Se) thin films," *Dalton Transactions*, vol. 47, no. 8, pp. 2628–2637, 2018.

[59] P. A. Ajibade and J. Osuntokun, "Synthesis and characterization of hexadecylamine capped ZnS, CdS, and HgS nanoparticles using heteroleptic single molecular precursors," *Journal of Nanomaterials*, vol. 2014, Article ID 782526, 7 pages, 2014.

[60] M. Wang, G. Yue, Y. Lin, X. Wen, D. Peng, and Z. Geng, "Synthesis, optical properties and photovoltaic application of the SnS quasi-one-dimensional nanostructures," *Nano-Micro Letters*, vol. 5, no. 1, pp. 1–6, 2013.

[61] O. Madelung, *Semiconductors—Basic Data*, Springer Science & Business Media, Berlin, Germany, 2012.

[62] S. C. Ray, M. K. Karanjai, and D. DasGupta, "Structure and photoconductive properties of dip-deposited SnS and SnS2 thin films and their conversion to tin dioxide by annealing in air," *Thin Solid Films*, vol. 350, no. 1-2, pp. 72–78, 1999.

[63] A. Kana, T. Hibbert, M. Mahon, K. Molloy, I. Parkin, and L. Price, "Organotin unsymmetric dithiocarbamates: synthesis, formation and characterisation of tin (II) sulfide films by atmospheric pressure chemical vapour deposition," *Polyhedron*, vol. 20, no. 24-25, pp. 2989–2995, 2001.

[64] K. Ramasamy, V. L. Kuznetsov, K. Gopal et al., "Organotin dithiocarbamates: single-source precursors for tin sulfide thin films by aerosol-assisted chemical vapor deposition (AACVD)," *Chemistry of Materials*, vol. 25, no. 3, pp. 266–276, 2013.

[65] C. Gao and H. Shen, "Influence of the deposition parameters on the properties of orthorhombic SnS films by chemical bath deposition," *Thin Solid Films*, vol. 520, no. 9, pp. 3523–3527, 2012.

[66] X. Zhao, S. Komuro, S. Fujita, H. Isshiki, Y. Aoyagi, and T. Sugano, "Size control of Si nanocrystallites formed in amorphous Si matrix by Er-doping," *Materials Science and Engineering: B*, vol. 51, no. 1-3, pp. 154–157, 1998.

[67] A. Phuruangrat, T. Thongtem, and S. Thongtem, "Synthesis of lead molybdate and lead tungstate via microwave irradiation method," *Journal of Crystal Growth*, vol. 311, no. 16, pp. 4076–4081, 2009.

[68] A. Stavrinadis, J. M. Smith, C. A. Cattley, A. G. Cook, P. S. Grant, and A. A. Watt, "SnS/PbS nanocrystal heterojunction photovoltaics," *Nanotechnology*, vol. 21, no. 18, article 185202, 2010.

[69] H. Gerung, S. D. Bunge, T. J. Boyle, C. J. Brinker, and S. M. Han, "Anhydrous solution synthesis of germanium nanocrystals from the germanium (II) precursor Ge [N $(SiMe_3)_2]_2$," *Chemical Communications*, vol. 14, pp. 1914–1916, 2005.

[70] M. Chen, Y.-G. Feng, X. Wang, T.-C. Li, J.-Y. Zhang, and D.-J. Qian, "Silver nanoparticles capped by oleylamine: formation, growth, and self-organization," *Langmuir*, vol. 23, no. 10, pp. 5296–5304, 2007.

[71] P. M. Shumbula, M. J. Moloto, T. R. Tshikhudo, and M. Fernandes, "Dichloro (bis [diphenylthiourea]) cadmium complex as a precursor for HDA-capped CdS nanoparticles and their solubility in water," *South African Journal of Science*, vol. 106, no. 7-8, pp. 1–7, 2010.

[72] N. Wu, L. Fu, M. Su, M. Aslam, K. C. Wong, and V. P. Dravid, "Interaction of fatty acid monolayers with cobalt nanoparticles," *Nano Letters*, vol. 4, no. 2, pp. 383–386, 2004.

[73] Y. Ren, K.-i. Iimura, and T. Kato, "Structure of barium stearate films at the air/water interface investigated by polarization modulation infrared spectroscopy and π–A isotherms," *Langmuir*, vol. 17, no. 9, pp. 2688–2693, 2001.